JOURNAL OF PROPULSION AND POWER
Vol. 27, No. 4, July–August 2011

Technical Notes

VX-200 Magnetoplasma Thruster Performance Results Exceeding Fifty-Percent Thruster Efficiency

Benjamin W. Longmier,* Leonard D. Cassady,† Maxwell G. Ballenger,‡ Mark D. Carter,§ Franklin R. Chang-Díaz,¶ Tim W. Glover,** Andrew V. Ilin,†† Greg E. McCaskill,‡‡ Chris S. Olsen,§§ and Jared P. Squire¶¶
Ad Astra Rocket Company, Webster, Texas 77598
and
Edgar A. Bering III***
University of Houston, Houston, Texas 77204

DOI: 10.2514/1.B34085

I. Introduction

HIGH-POWER electric propulsion thrusters can reduce propellant mass for heavy-payload orbit-raising missions and cargo missions to the moon and near-Earth asteroids, and they can reduce the trip time of robotic and piloted planetary missions [1–4]. The Variable Specific Impulse Magnetoplasma Rocket (VASIMR®) VX-200 engine is an electric propulsion system capable of processing power densities on the order of 6 MW/m^2 with a high specific impulse (4000 to 6000 s) and an inherent capability to vary the thrust and specific impulse at a constant power. The potential for a long lifetime is due primarily to the radial magnetic confinement of both ions and electrons in a quasi-neutral flowing plasma stream, which acts to significantly reduce the plasma impingement on the walls of the rocket core. High-temperature ceramic plasma-facing surfaces handle the thermal radiation: the principal heat transfer mechanism from the discharge. The rocket uses a helicon plasma source [5,6] for efficient plasma production in the first stage. This plasma is energized further by an ion cyclotron heating (ICH) RF stage that uses left-hand polarized slow-mode waves launched from the high field side of the ion cyclotron resonance. Useful thrust is produced as the plasma accelerates in an expanding magnetic field: a process described by conservation of the first adiabatic invariant as the magnetic field strength decreases in the exhaust region of the VASIMR [7–9].

End-to-end testing of the VX-200 engine has been undertaken with an optimum magnetic field and in a vacuum facility with sufficient volume and pumping to permit exhaust plume measurements at low background pressures. Experimental results are presented with the VX-200 engine installed in a 150 m^3 vacuum chamber with an operating pressure below 1×10^{-2} Pa (1×10^{-4} torr), and with an exhaust plume diagnostic measurement range of 5 m in the axial direction and 1 m in the radial directions. Measurements of plasma flux, RF power, and neutral argon gas flow rate, combined with knowledge of the kinetic energy of the ions leaving the VX-200 engine, are used to determine the ionization cost of the argon plasma. A plasma momentum flux sensor (PMFS) measures the force density as a function of radial and axial positions in the exhaust plume. New experimental data on ionization cost, exhaust plume expansion angle, thruster efficiency, and total force are presented that characterize the VX-200 engine performance above 100 kW. A semi-empirical model of the thruster efficiency as a function of specific impulse has been developed to fit the experimental data, and an extrapolation to 200 kW dc input power yields a thruster efficiency of 61% at a specific impulse of 4800 s.

II. Experimental Setup and Method

A. VX-200 Engine

The VX-200 engine is an experimental VASIMR prototype designed to operate at 200 kW of input dc electrical power. The device provides an end-to-end integrated test of the primary VASIMR components in a vacuum environment, with the goal of measuring and improving the system performance. A majority of the VX-200 engine components are located within the vacuum chamber, with only the solid-state RF generators, superconducting magnet power supplies, and cryocoolers kept at atmospheric pressure.

The superconducting magnet, structural, rocket core, engine sensors, and electrical components are operated within the vacuum chamber. Figure 1 shows a schematic of the VX-200 engine installed inside the vacuum chamber and the approximate shape of the magnetic field flux lines within the core and magnetic nozzle.

The core of the VX-200 engine is defined as the components that physically surround the plasma and intercept the bulk of the waste heat radiated by the plasma column. The VX-200 engine is restricted to pulses of less than 1 min, owing to temperature limitations of certain seals and joints in the rocket core. The helicon stage launches a right-handed circularly polarized wave, which produces a cold argon plasma. A pressure gradient drives the plasma flow through a magnetic choke into the ICH stage, where another RF coupler launches a wave that preferentially heats the ions in a single pass [9].

The VX-200 engine RF generators convert facility dc power to RF power and perform impedance matching between the RF generator output and the rocket core. The RF generators were custom built by Nautel, Ltd., model numbers VX200-1 (helicon generator) and VX200-2 (ICH generator). The VX200-1 RF generator is rated up to 48 ± 1 kW RF, with a $91 \pm 1\%$ efficiency and a specific mass of 0.85 ± 0.02 kg/kW. The VX200-2 generator is rated up to 172 ± 1 kW RF, with a $98 \pm 1\%$ efficiency and a specific mass of 0.506 ± 0.003 kg/kW. The generator efficiencies were determined by independent testing performed by Nautel, Ltd., which included a direct measurement of input power and calorimetry of the dissipated power in the generator.

The exhaust velocity of the ions increases as the coupled ICH power increases. Coupled RF power is defined as the RF power that is injected by the helicon and/or ICH couplers and is inductively absorbed by the plasma column or radiatively lost by the RF

Received 12 August 2010; revision received 1 February 2011; accepted for publication 24 February 2011.

*Principal Research Scientist; ben.longmier@adastrarocket.com. Member AIAA.
†Lead Engineer; lcassady@adastrarocket.com. Member AIAA.
‡Staff Scientist; maxwell.ballenger@adastrarocket.com.
§Director of Technology; mark.carter@adastrarocket.com. Member AIAA.
¶Chief Executive Officer;, aarc@adastrarocket.com. Associate Fellow AIAA.
**Director of Development; tim.glover@adastrarocket.com. Member AIAA.
††Computational Research Lead; andrew.ilin@adastrarocket.com.
‡‡Senior RF Engineer; greg.mccaskill@adastrarocket.com.
§§Research Scientist; chris.olsen@adastrarocket.com.
¶¶Director of Research; jared.squire@adastrarocket.com. Member AIAA.
***Professor, Departments of Physics and Electrical and Computer Engineering; eabering@uh.edu. Associate Fellow AIAA.

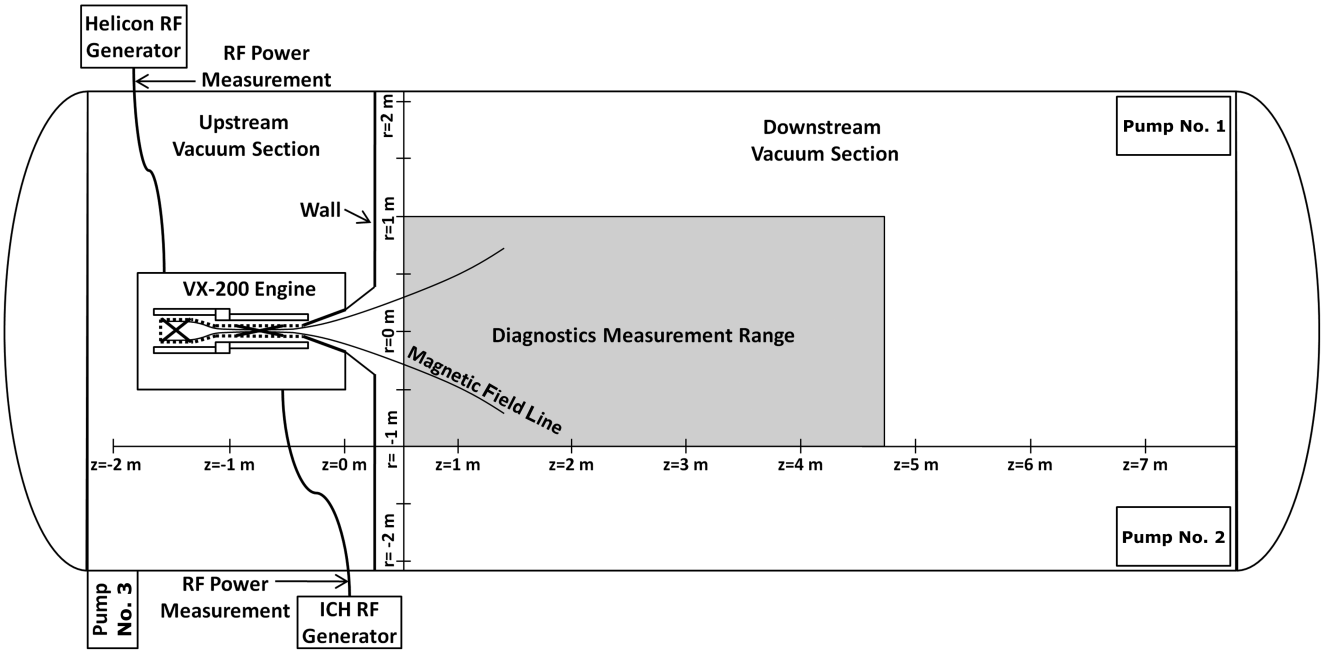

Fig. 1 Schematic of 10 × 4.2 m chamber with VX-200 engine, RF generators, RF power measurement location, vacuum partitioning wall, representative magnetic field lines, and measurement range of exhaust plume diagnostics.

couplers. The coupled RF power is determined by subtracting the power losses in the RF matching network and RF transmission line from the measured RF power at the RF generator output; see Fig. 1. Losses in the matching networks and transmissions lines are calculated based on network analyzer measurements of circuit impedance, and they were determined to be 96% efficient for both the helicon and ICH RF circuits.

The VX-200 engine low-temperature superconducting (LTSC) magnet is cooled to 6 K by Sumitomo cryocooler (RDK-408D2)/ cryocompressor (CSW-71) units with a maximum combined power draw of 15 kW. The VX-200 engine LTSC magnet produces a maximum magnetic field strength of 2 T that results in highly confined electrons and argon ions within the engine core. Estimates for cryocooler power draw for flight designs are less than 3 kW total for high-temperature superconducting magnets cooled to 50 K. The magnetic field in the VX-200 engine is responsible for efficient ion cyclotron coupling of the RF energy to the ions within the quasi-neutral flowing plasma. The applied expanding magnetic field converts perpendicular ion kinetic energy $E_\perp$ to directed parallel ion kinetic energy $E_\parallel$ through conservation of the magnetic moment and conservation of the ion's total kinetic energy [7–9]. The location at which 90% of the perpendicular ion energy is converted into parallel ion energy, $E_\parallel/E_\perp = 90\%$, occurs at $z = 5$ cm.

An ambipolar ion acceleration has also been observed [10] and is believed to be the result of the plasma interaction with the magnetic field gradient in the expanding magnetic nozzle of the VX-200 engine, similar to the Boltzman relation but with a varying electron temperature. The ambipolar ion acceleration typically results in an additional directed ion velocity of 5 to 10 km/s, where the energy for this process comes from the electron energy distribution function as a result of electron and ion interaction with a weak electric field in the magnetic nozzle, which ranges in strength from 10 to 20 V/m, depending on system parameters.

The data presented in this paper were taken during quasi-steady-state operation, up to 30 s in duration. The neutral pressure gradients within the VX-200 engine and the vacuum system equalize within 0.8 s of the initial startup. From 0.8 through 30 s, the neutral pressure throughout the VX-200 engine and vacuum systems are steady-state values. Data for the thruster efficiency calculations were taken during the steady-state portion of the VX-200 operation. The propellant mass flow rate can be varied between 50 to 150 mg/s and was measured by use of a calibrated proportional flow control valve flow controller in addition to a calibrated [National Institute of Standards and Technology (NIST) traceable] thermal-based mass flowmeter that was inline at the high-pressure end of the propellant feed system.

B. Vacuum Facility

The VX-200 engine is installed, as shown in Fig. 1, inside a stainless steel vacuum chamber [11,12] that is 4.2 m in diameter and 10 m long, with a volume of 150 m^3, including the end caps. One end opens fully for access to the entire inner diameter of the chamber. The vacuum chamber is partitioned into two sections: an upstream section and a downstream section. The upstream vacuum section (where the VX-200 engine is located) is kept at a pressure one to two orders of magnitude lower than the downstream, or exhaust, vacuum section while the VX-200 is firing. The partition, located at $z = 20$ cm, helps to prevent arcing and glow discharges near the high-voltage transmission lines and matching circuit components. Similar work related to the challenges of operating a RF antenna in vacuum was performed by West et al. [13]. The facility used two PHPK Technologies CVI Torr Master internal cryopumps in the downstream section of the vacuum chamber and provided an Ar pumping speed of ∼100, 000 l/s. The exhaust section pressure was less than 1×10^{-3} Pa (1×10^{-5} torr) for the first 0.8 s, and it was less than 1×10^{-2} Pa (1×10^{-4} torr) from 0.8 to 30 s of operation, yielding a charge exchange mean free path of ∼100 and ∼10 cm, respectively. The base pressure of the vacuum chamber was less than 7×10^{-6} Pa (5×10^{-8} torr) before each shot.

C. Flux Probe Array

The ion flux was measured with an array of 10 0.64-cm-diam molybdenum planar probes, of a top hat design [14], that were biased into the ion saturation regime of −15 V with respect to chamber ground. Full current-voltage traces were taken with a Langmuir probe of the same dimensions and analyzed to ensure that the ion flux probes were biased $3T_e$ more negative than the floating potential. Ion flux measurements were taken both during quick startup shots, where the ambient neutral gas pressure was below 1×10^{-3} Pa (1×10^{-5} torr), and during translating radial profiles, where the sustained neutral argon pressure within the vacuum chamber was 1×10^{-2} Pa (1×10^{-4} torr).

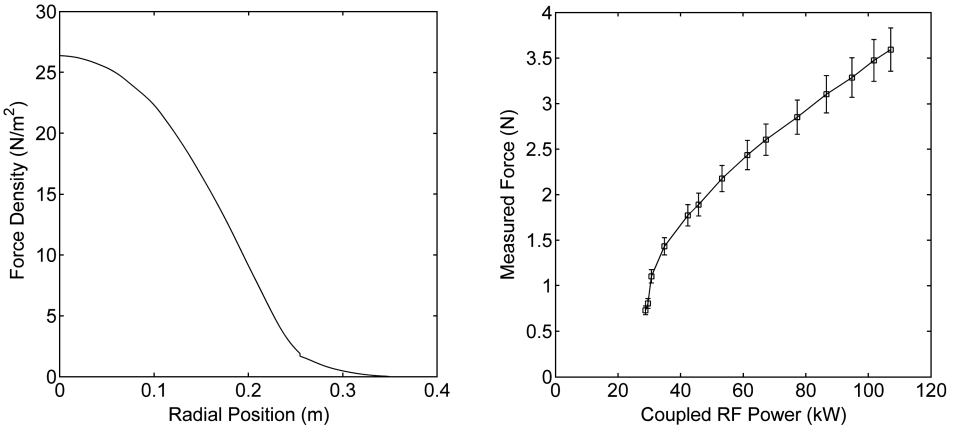

Fig. 2 VX-200 engine: a) measured radial profile of force density and b) total force as a function of RF power coupled to argon plasma. Error in Fig. 2a is 7% of force density value.

D. Plasma Momentum Flux Sensor

A PMFS, which has been described in detail elsewhere [15], was used to measure the force of the plasma ejected from the VX-200 engine. The PMFS consists of a 9-cm-diam electrically floating graphite target disk that is attached to a stiff 10-cm-long insulating alumina rod. The stiff alumina rod connected to a small titanium bar (5.72 by 1.30 cm), where a series of four high-output semiconductor strain gauges measured the strain caused by the torque from the applied plasma impact force. The PMFS was calibrated with the method employed by Chavers and Chang-Díaz [16,17]. A small graphite shield was used to shield the entire titanium bar and strain gauge assembly from the flowing plasma stream.

The resolution of the PMFS was 0.1 mN, which allowed for sufficiently sensitive measurements of the force applied by the exhaust plasma. The natural frequency of oscillations was 40 Hz, and this oscillation was filtered out during the analysis of radial or temporal force profiles, although the temporal data are limited in resolution to $\sim 1/40$ s. The use of the PMFS technique was previously compared and validated with a more traditional inverted pendulum thrust stand in a 9-m-long 6-m-diam vacuum chamber using the P5 Hall thruster [15]. Other groups have employed similar PMFSs, the use of which has been promising due to size, cost, and configuration limitations commonly associated with thrust stands [18–27].

E. Retarding Potential Analyzer

Measurements of the ion energy in the exhaust region were made with a four-grid retarding potential analyzer (RPA) [9]. The grids were 49.2-wire/cm nickel mesh and spaced 1 mm apart with Macor spacers. The opening aperture was 1 cm in diameter and usually centered on the VX-200 engine axis. A four-grid configuration was used, with entrance attenuator, electron suppressor, ion analyzer, and secondary suppressor grids. The ion exhaust velocity was deduced from the raw data by means of least-squares fits of drifting Maxwellians to the current-voltage data from the RPA [28–31]. RPAs work by varying a repelling potential on the ion analyzer grid. Ions with a flow kinetic energy greater than the retarding electrostatic potential energy reach the collector. Since multiply ionized ions do not have the same ion cyclotron frequency, they will have a very different energy distribution and flow velocity than the singly ionized ions that are accelerated by the ICH stage of the VX-200 engine. Multiple component ion populations appear in RPA data as a stepped current-voltage characteristic, which must be analyzed by fitting a multicomponent distribution. Previous studies of a 10%-deuterium 90%-hydrogen plasma in a VASIMR device have demonstrated that a plasma with a 10% component with a factor of two different m/q ratios can easily be resolved [32]. Based on these prior results, it is a conservative estimate that the RPA would have seen a resolvable second lower energy Maxwellian population with a detection level of 5% of the singly ionized Maxwellian population [32].

F. Optical Spectrometer

Data from an Ocean Optics USB4000 fiber optic spectrometer were used to look for spectral emission lines from neutral argon (ArI), singly ionized argon (ArII), doubly ionized argon (ArIII), triply ionized argon (ArIV), and trace impurities in the plume at $z = 5$ cm and $r = 0$ cm. The spectrometer had a range of 200 to 1100 nm, with a resolution of 0.3 nm. The spectrometer used a 2 deg collimation lens and looked through the diameter of the exhaust plume at a matte black plate on the far side of the plume, which was used to absorb reflected light from stray sources. The NIST atomic spectra database was used to identify ArI, ArII, ArIII, ArIV, and other spectral lines.[†††]

III. Experimental Results and Discussion

For the first time, the total force from the VASIMR VX-200 engine has been measured. Using the PMFS, the force density within the exhaust plume of the VX-200 engine was measured as a function of the radial and axial positions. To determine the total force produced by the VX-200 engine, the force density over one full radius of the exhaust plume, as shown in Fig. 2a, was integrated using azimuthal symmetry. As the coupled RF power was increased from 28 to 108 kW, the total force produced by the VX-200 engine was measured using the PMFS. As shown in Fig. 2b, the total force measured increased with increasing ICH coupled RF power as expected.

For the data presented in Figs. 2a and 2b, the PMFS was located at $z = 40$ cm, where $E_{\parallel}/E_{\perp} = 98\%$. The PMFS was 9 cm in diameter, which is small compared with the total exhaust plume diameter of approximately 70 cm. The force density data for Fig. 2a were taken radially at 14 samples/cm from $r = 0$ cm to $r = 40$ cm, and one sample was taken axially every 10 cm from $z = 40$ cm to $z = 150$ cm. The VX-200 engine was operated with 107 mg/s of Ar propellant, a peak magnetic field strength of 2 T, a helicon coupled RF power level of 28 kW, and an ICH coupled RF power level of 90 kW for the data presented in Fig. 2a, and an ICH power level from 0 to 81 kW for the data presented in Fig. 2b.

No indication of secondary (Ar^{2+}) or tertiary (Ar^{3+}) ionization states were observed based on optical spectrometer measurements 30 cm downstream of the VX-200 engine exit plane. This implies that the population of Ar^{2+} and Ar^{3+} ions is at least less than 1% of the Ar^{+} population. In addition, Ar^{2+} and Ar^{3+} ions are not detected to

[†††]Data available at http://physics.nist.gov/cgi-bin/AtData/lines_form [retrieved 26 January 2011].

within 5% of the Ar^+ population based on RPA data at a location of $z = 40$ cm. For the data presented in Fig. 2a, the ion-neutral charge exchange mean free path was 10 cm, and for Figs. 2b and 3, it was 100 cm, since the data were taken within the first 800 ms of operation.

The ion current density and force density were mapped over a large region of the exhaust plume ($z = 40$ cm to 260 cm axially with a resolution of 10 cm, and $r = 0$ to ± 75 cm radially with a resolution of 0.7 mm), with the flat faces of the ion current density probes and the PMFS always in a plane orthogonal to the VX-200 engine axis, i.e., always facing in the direction parallel to the engine axis. This mapping was performed at a total coupled RF power level of 90 kW and a neutral background pressure of 1×10^{-2} Pa (1×10^{-4} torr). The plasma jet data exhibited a well-defined edge in both ion current density and force density [11], similar to other helicon-based devices [33]. Assuming azimuthal symmetry, the conical boundary contour that surrounded 90% of the integrated ion current density and force density was calculated. The angle of that boundary line relative to the VX-200 engine axis θ provided an estimate of the exhaust divergence half-angle. The ion current density data yielded a divergence half-angle of 30 ± 2 deg, while the force density data yielded a divergence half-angle of 24 ± 2 deg. The half-angles were found by radially integrating the ion current density and force density to 90% of the total ion current and total force. The ion flux probe and the PMFS were not rotated such that the ions impacted normal to these surfaces, but they were left facing in the direction parallel to the VX-200 engine centerline and translated radially. The conical nozzle correction factor [34] can be used to estimate the fraction of directed momentum to total flow momentum. Here, this correction factor is defined as the nozzle efficiency when expressed as a percentage,

$$\eta_n = \tfrac{1}{2}(1 + \cos\theta) \tag{1}$$

The integrated current density and force density data yield a nozzle efficiency of 93 and 96%, respectively. For the following system efficiency analysis, the more conservative 93% nozzle efficiency was used. This estimate was consistent with particle trajectory modeling [35] that predicted a nozzle efficiency of 90%. Calculations based on a magnetohydrodynamics theory [36] that factors in possible drag effects due to the plasma leaving the high magnetic strength zone yield a nozzle efficiency of 87%.

The total thruster efficiency η_T of the VX-200 engine was determined by dividing the total RF power coupled to the plasma by the thruster jet power, where the jet power is defined as

$$P_{\text{jet}} = \frac{F^2}{2\dot{m}} \tag{2}$$

where F is the total force produced by the rocket and $\dot{m}$ is the total mass flow rate of propellant. Dividing Eq. (2) by the total RF power coupled to the plasma yields

$$\eta_T = \frac{P_{\text{jet}}}{P_{1,\text{RF}} + P_{2,\text{RF}}} \tag{3}$$

where $P_{1,\text{RF}}$ and $P_{2,\text{RF}}$ represent the RF power coupled to the helicon and ICH stages of the VX-200 engine, respectively.

Figure 3 shows the total thruster efficiency as a function of the specific impulse, where the specific impulse was calculated using Eq. (4) with measured values of force (Fig. 2b) and propellant flow rate, and the total thruster efficiency was calculated using Eq. (3). For data presented in Fig. 3, the VX-200 engine used a propellant flow rate of 107 mg/s, a helicon coupled RF power level of 28 kW, and an ICH coupled RF power level from 0 to 81 kW, which yielded results that show a total force of up to 3.6 ± 0.2 N, at an I_{sp} of 3400 s, and a 56% thruster efficiency. The RPA was used to verify the PMFS results and reported a mean ion flow velocity of 32.8 km/s with an ion temperature of 24 eV in the frame of reference moving with the beam. Solving for force in Eq. (4), and using a propellant mass flow rate of 107 mg/s and a mean ion velocity of 32.8 km/s, the RPA measurements indicate a total calculated force of 3.5 ± 0.5 N, within the error bars of the PMFS force measurement of 3.6 ± 0.2 N:

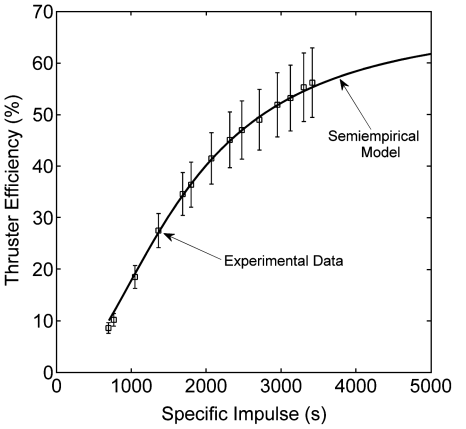

Fig. 3 Thruster efficiency of VX-200 engine as a function of specific impulse.

$$I_{\text{sp}} = \frac{F}{\dot{m}g} \tag{4}$$

Any change to the thruster efficiency was due largely to the increasing component of ICH coupled RF power. The limiting factor in the maximum ICH coupled RF power to the VX-200 engine was a vacuum pressure limit within the vacuum chamber, where greater RF circuit voltages produced glow or arc discharges that prompted the VX-200 engine solid-state RF generators to shut down. The total thruster efficiency in Fig. 3 increases as a function of coupled ICH RF power and I_{sp}, indicating that the process of ICH wave coupling into the plasma column has not saturated.

Measurements of the ionization cost, defined as the ratio of the coupled RF power to the total ion current that is extracted from the system in the exhaust section, were taken during helicon-only operation as a function of both coupled RF power and argon propellant flow rate, from 15 to 35 kW and 50 to 150 mg/s, respectively. The lowest ionization cost measurement of 87 ± 9 eV occurred with VX-200 engine settings of 28 kW coupled RF power and 130 mg/s argon flow rate. The ionization cost term E_i appears in Eq. (5). Although a small fraction of ICH power may be absorbed by electrons, for the purposes of the semiempirical model in Fig. 3 and Eq. (5), it is assumed that the ICH process does not affect E_i.

A semiempirical model of the thruster efficiency [11,23] for the VX-200 engine [Eq. (5)] is also shown in Fig. 3, and it is a least-squares fit to the data using the ICH coupling efficiency as the only free parameter, such that

$$\eta_T = \frac{1}{2} m_{\text{Ar}} g^2 I_{\text{SP}}^2 \Big/ \left[eE_i + eE_1\left(1 - \frac{1}{\eta_B}\right) + \frac{(1/2) m_{\text{Ar}} g^2 I_{\text{SP}}^2}{\eta_B \eta_n} \right] \tag{5}$$

where m_{Ar} is the atomic mass of argon, g is the gravitational acceleration, I_{SP} is the specific impulse, e is the electron charge, E_i is the ionization cost of the propellant, E_1 is the first-stage (helicon) RF power coupled to the plasma that is converted into directed ion kinetic energy through ambipolar acceleration, η_B is the ICH efficiency, and η_n is the nozzle efficiency. The ionization cost of the propellant was $E_i = 87 \pm 9$ eV/ion-extracted, the kinetic energy of ions leaving the first stage was $E_1 = 12 \pm 1$ eV, and the nozzle efficiency was $\eta_n = 93\%$. The only free parameter was the ICH coupling efficiency η_B, which was fit to the data using a least-squares algorithm (as shown in Fig. 3), and it was found to be 74%. It should be noted that η_B also includes the efficiency loss due to the ion energy spread in the exhaust, i.e., the frozen flow losses due to the finite ion temperature. Decreasing E_i or increasing E_1 shifts the semiempirical model curve to the left, and increasing η_B or η_N shifts the curve upward. The VX-200 engine helicon and ICH couplers were designed to produce a thruster efficiency of 60% at 5000 s using 200 kW dc input power (equivalent to 186 kW of coupled helicon and ICH RF power). Extrapolating the measured thruster efficiency using the semiempirical model suggests that the VX-200 engine would

achieve a thruster efficiency of 61% at 4800 s using 200 kW of dc input power.

IV. Conclusions

For the first time, the thruster efficiency and the thrust of a high-power VASIMR prototype have been measured with the thruster installed inside a vacuum chamber with sufficient volume and pumping to simulate the vacuum conditions of space. Using an ion flux probe array and a PMFS, the exhaust of the VX-200 engine was characterized as a function of the coupled RF power and as a function of the radial and axial positions within the exhaust plume. A thruster efficiency of 56% was calculated using the force measurements and propellant flow rate with the specific impulse of 3400 s when operating at a total RF coupled power of 108 kW. The ionization cost of argon propellant was determined to be 87 eV for optimized values of RF power and propellant flow rate. Using a semiempirical model, it is predicted that the VX-200 engine will have a thruster efficiency of 61% at 4800 s when operated at 200 kW dc input power. Experiments are ongoing, as the VX-200 will be operated at up to 200 kW of input dc power with a new ICH coupler to confirm the predicted efficiency at high I_{sp}. This work paves the way for design and eventual operation of a VASIMR engine in orbit onboard the International Space Station.

References

[1] Frisbee, R., "SP-100 Nuclear Electric Propulsion for Mars Cargo Missions," 29th AIAA/SAE/ASME/ASEE Joint Propulsion Conference, Monterey, CA, AIAA Paper 1993-2092, June 1993.

[2] Frisbee, R., "Electric Propulsion Options for Mars Cargo Missions," 32nd AIAA/ASME/SAE/ASEE Joint Propulsion Conference and Exhibit, Lake Buena Vista, FL, AIAA Paper 1996-3173, July 1996.

[3] Sankaran, K., Cassady, L., Kodys, A., and Choueiri, E., "A Survey of Propulsion Options for Cargo and Piloted Missions to Mars," *Annals of the New York Academy of Sciences*, Vol. 1017, 2004, pp. 450–567. doi:10.1196/annals.1311.027

[4] Ilin, A., Cassady, L., Glover, T., Carter, M., and Chang Díaz, F., "A Survey of Missions Using VASIMR for Flexible Space Exploration," NASA, TR JSC-65825, April 2010.

[5] Boswell, R. W., and Chen, F. F., "Helicons: The Early Years," *IEEE Transactions on Plasma Science*, Vol. 25, No. 6, Dec. 1997, pp. 1229–1244. doi:10.1109/27.650898

[6] Chen, F. F., and Boswell, R. W., "Helicons: The Past Decade," *IEEE Transactions on Plasma Science*, Vol. 25, No. 6, Dec. 1997, pp. 1245–1257. doi:10.1109/27.650899

[7] Northrop, T. G., "The Adiabatic Motion of Charged Particles," *American Journal of Physics*, Vol. 32, No. 10, 1964, pp. 807–807. doi:10.1119/1.1969867

[8] Roederer, J. G., "Dynamics of Geomagnetically Trapped Radiation," *Physics and Chemistry in Space*, Springer, Berlin, 1970, pp. 1–19.

[9] Bering, E. A., III, Chang Díaz, F. R., Squire, J. P., Glover, T. W., Carter, M. D., McCaskill, G. E., Longmier, B. W., Brukardt, M. S., Chancery, W. J., and Jacobson, V. T., "Observations of Single-Pass Ion Cyclotron Heating in a Trans-Sonic Flowing Plasma," *Physics of Plasmas*, Vol. 17, No. 4, 2010, Paper 043509. doi:10.1063/1.3389205

[10] Longmier, B., Bering, E., Carter, M., Cassady, L., Chancery, W., Chang Díaz, F., Glover, T., Hershkowitz, N., Ilin, A., McCaskill, G., Olsen, C., and Squire, J., "Ambipolar Ion Acceleration in an Expanding Magnetic Nozzle," *Plasma Sources Science and Technology* , Vol. 20, No. 1, 2011, Paper 015007. doi:10.1088/0963-0252/20/1/015007

[11] Cassady, L. D., Longmier, B. W., Olsen, C. S., Ballenger, M. G., McCaskill, G. E., Ilin, A. V., Carter, M. D., Glover, T. W., Squire, J. P., and Chang Díaz, F. R., "VASIMR Performance Results," 46th AIAA/ASME/SAE/ASEE Joint Propulsion Conference and Exhibit, Nashville, TN, AIAA Paper 2010-6772, July 2010.

[12] Longmier, B. W., Bering, E. A., Squire, J. P., Glover, T. W., Chang Diaz, F. R., and Brukardt, M., "Exhaust Plume Measurements of the VASIMR VX-200," *Bulletin of the American Physical Society*, Vol. 53, No. 14, 2008, p. 216.

[13] West, M., Charles, C., and Boswell, R., "Operating Radio Frequency Antennas Immersed in Vacuum: Implications for Ground-Testing Plasma Thrusters," *Journal of Propulsion and Power*, Vol. 26, No. 4, 2010, pp. 892–896. doi:10.2514/1.49384

[14] Olsen, C., "Ion Flux Maps and Helicon Source Efficiency in the VASIMR VX-100 Experiment Using a Moving Langmuir Probe Array," M.S. Thesis, Rice Univ., Houston, TX, Feb. 2009.

[15] Longmier, B., Reid, B., Gallimore, A., Chang Díaz, F., Squire, J., Glover, T., Chavers, G., and Bering, E., "Validating a Plasma Momentum Flux Sensor to an Inverted Pendulum Thrust Stand," *Journal of Propulsion and Power*, Vol. 25, No. 3, May–June 2009, pp. 746–752. doi:10.2514/1.35706

[16] Chavers, G., and Chang-Díaz, F., "Momentum Flux Measuring Instrument for Neutral and Charged Particle Flows," *Review of Scientific Instruments*, Vol. 73, No. 10, 2002, Paper 3500. doi:10.1063/1.1505107

[17] Chavers, G., Chang-Diaz, F., Irvine, C., and Squire, J., "Momentum and Heat Flux Measurements Using an Impact Target in Flowing Plasma," *Journal of Propulsion and Power*, Vol. 22, No. 3, 2006, pp. 637–644. doi:10.2514/1.1971

[18] Yanagi, R., and Kimura, I., "New Type of Target for the Measurement of Impulse Bits of Pulsed Plasma Thrusters," *Journal of Spacecraft and Rockets*, Vol. 19, No. 3, 1982, pp. 246–249. doi:10.2514/3.62245

[19] Grun, J., and Ripin, B., "Ballistic Pendula for Measuring the Momentum of a Laser- Produced Plasma," *Review of Scientific Instruments*, Vol. 53, No. 12, 1982, pp. 1878–1881. doi:10.1063/1.1136897

[20] Cohen, S., Zonca, F., Timberlake, J., Bennett, T., Cuthbertson, J., Langer, W., and Motley, R., "An Instrument for Measuring the Momentum Flux From Atomic and Charged Particle Jets," *Review of Scientific Instruments*, Vol. 61, No. 11, 1990, pp. 3586–3591. doi:10.1063/1.1141575

[21] Takao, Y., Eriguchi, K., and Ono, K., "A Miniature Electrothermal Thruster Using Microwave-Excited Microplasmas: Thrust Measurement and its Comparison with Numerical Analysis," *Journal of Applied Physics*, Vol. 101, No. 12, 2007, Paper 123307. doi:10.1063/1.2749336

[22] Lunt, T., Silva, S., Fernandes, H., Hidalgo, C., Pedrosa, M. A., Duarte, P., Figueiredo, H., and Pereira, T., "Edge Plasma Pressure Measurements Using a Mechanical Force Sensor on the Tokamak ISTTOK," *Plasma Physics and Controlled Fusion*, Vol. 49, No. 11, 2007, pp. 1783–1790. doi:10.1088/0741-3335/49/11/003

[23] Böhrk, H., and Auweter-Kurtz, M., "Thrust Measurement of the Hybrid Electric Thruster TIHTUS by a Baffle Plate," *Journal of Propulsion and Power*, Vol. 25, No. 3, 2009, pp. 729–736. doi:10.2514/1.34324

[24] West, M., Charles, C., and Boswell, R., "A High Sensitivity Momentum Flux Measuring Instrument for Plasma Thruster Exhausts And Diffusive Plasmas," *Review of Scientific Instruments*, Vol. 80, No. 5, 2009, Paper 053509. doi:10.1063/1.3142477

[25] Makrinich, G., and Fruchtman, A., "Experimental Study of a Radial Plasma Source," *Physics of Plasmas*, Vol. 16, No. 4, 2009, Paper 043507. doi:10.1063/1.3119688

[26] Ling, J., West, M., Lafleur, T., Charles, C., and Boswell, R., "Thrust Measurements in a Low-Magnetic Field High-Density Mode in the Helicon Double Layer Thruster," *Journal of Physics. D. Applied Physics*, Vol. 43, No. 30, 2010, Paper 305203. doi:10.1088/0022-3727/43/30/305203

[27] Chen, X., "The Impact Force Acting on a Flat Plate Exposed Normally to a Rarefied Plasma Plume Issuing From an Annular or Circular Nozzle," *Journal of Physics. D. Applied Physics*, Vol. 43, No. 31, 2010, Paper 315205. doi:10.1088/0022-3727/43/31/315205

[28] Whipple, E. C., "The Ion Trap-Results in 'Exploration of the Upper Atmosphere with the Help of the Third Soviet Sputnik'," *Proceedings of the IRE*, Vol. 47, 1959, pp. 2023–2024.

[29] Parker, L. W., and Whipple, E. C., "Theory of Spacecraft Sheath Structure, Potential, and Velocity Effects on Ion Measurements by Traps and Mass Spectrometers," *Journal of Geophysical Research*, Vol. 75, No. 25, 1970, pp. 4720–4733. doi:10.1029/JA075i025p04720

[30] Minami, S., and Takeya, Y. J., "Ion Temperature Determination in the Ionosphere by Retarding Potential Analyzer Aboard Sounding Rocket," *Journal of Geophysical Research*, Vol. 87, No. , 1982, pp. 713–730. doi:10.1029/JA087iA02p00713

[31] Hutchinson, I. H., *Principles of Plasma Diagnostics*, Cambridge Univ. Press, Cambridge, MA, 1987, pp. 94–99.
[32] Bering, E. A., III., Chang Díaz, F. R., and Squire, J. P., "The Uses of RF Waves in Space Propulsion Systems," *Radio Science Bulletin* Vol. 310, 2004, pp 92–106.
[33] Cox, W., Charles, C., Boswell, R., and Hawkins, R., "Spatial Retarding Field Energy Analyzer Measurements Downstream of a Helicon Double Layer Plasma," *Applied Physics Letters*, Vol. 93, No. 7, 2008, Paper 071505.
doi:10.1063/1.2965866
[34] Sutton, R., and Biblarz, O., *Rocket Propulsion Elements*, 7th ed., Wiley, New York, 2001, pp. 75–78.
[35] Ilin, A., Chang Díaz, F., Squire, J., Tarditi, A., Breizman, B., and Carter, M., "Simulations of Plasma Detachment in VASIMR," 40th AIAA Aerospace Sciences Meeting and Exhibit, Reno, NV, AIAA Paper 2002-0346, Jan. 2002.
[36] Arefiev, A., and Breizman, B., "Magnetohydrodynamic Scenario of Plasma Detachment in a Magnetic Nozzle," *Physics of Plasmas*, Vol. 12, 2005, Paper 043504.
doi:10.1063/1.1875632

A. Gallimore
Associate Editor